Effects of Mn substitution on thermoelectric properties of $CuIn_{1-x}Mn_xTe_2$*

Pengfei Luo(罗鹏飞)[1,2], Li You(游理)[3], Jiong Yang(杨炯)[2], Juanjuan Xing(邢娟娟)[3], Jiye Zhang(张继业)[3], Chenyang Wang(王晨阳)[3], Xinluo Zhao(赵新洛)[1], Jun Luo(骆军)[3,†] and Wenqing Zhang(张文清)[2,3,‡]

[1] *Department of Physics, Institute of Low-Dimensional Carbons and Device Physics, Shanghai University, Shanghai* 200444, *China*

[2] *Materials Genome Institute, Shanghai University, Shanghai* 200444, *China*

[3] *School of Materials Science and Engineering, Shanghai University, Shanghai* 200444, *China*

(Received 8 May 2017; revised manuscript received 10 June 2017; published online 27 July 2017)

$CuIn_{1-x}Mn_xTe_2$ samples have been synthesized by a melt-annealing method. The x-ray powder diffraction (XRD) analysis shows that the $CuIn_{1-x}Mn_xTe_2$ samples crystallize in the chalcopyrite phase. Mn doping can effectively optimize the electrical properties and accordingly improve the power factor. The room temperature electrical conductivity of doped $CuInTe_2$ increases by several orders of magnitude due to substituting In with Mn. In addition, a large reduction in thermal conductivity is achieved through the enhanced phonon scattering via Mn-related point defects and precipitates. Therefore, an enhanced average ZT value up to 0.34 is achieved for sample $CuIn_{0.925}Mn_{0.075}Te_2$, which is 41% higher than that of the pristine $CuInTe_2$.

Keywords: thermoelectrics, chalcopyrite, $CuInTe_2$, Mn doping

PACS: 72.15.JF, 74.25.fg **DOI:** 10.1088/1674-1056/26/9/097201

1. Introduction

Thermoelectric conversion technology, which could convert heat into electricity for power generation or vice versa convert electrical energy into heat for refrigeration, provides a possible solution for the energy shortage and environmental concerns.[1–3] However, the low conversion efficiency limits the large-scale application of thermoelectric technology, which is determined by the dimensionless thermoelectric figure-of-merit (ZT). ZT is defined as $ZT = S^2\sigma T/\kappa$, where S is the Seebeck coefficient, σ the electric conductivity, T the absolute temperature, and κ the thermal conductivity, respectively.

Recently, much effort has been focused on ternary *I–III–VI*2-type (I = Cu, Ag; III = Al, Ga, In; and VI = S, Se, Te) chalcopyrite compounds owing to their nontoxicity, low lattice thermal conductivity, and good electrical transport properties.[4–13] So far, many compounds with high ZT values have been reported, for example, $CuGaTe_2$ with a ZT value of 1.4,[14] $Ag_{0.95}GaTe_2$ with a ZT value of 0.77,[15] $Cu_{1-x}Mn_xInTe_2$ with a ZT value of 0.84[16] and $CuInTe_{1.99}Sb_{0.01}$ + 1 wt% ZnO system with a ZT value of 1.61.[4] Among these ternary chalcopyrite compounds, p-type $CuInTe_2$ are characterized by relatively high Seebeck coefficient and low high-temperature thermal conductivity, owing to its degenerate valence bands[4] and highly distorted crystal structure,[7] respectively, which makes it a promising high-temperature thermoelectric material. Nevertheless, the further application of un-doped $CuInTe_2$ is still retarded by its poor electrical conductivity and high room-temperature thermal conductivity. Therefore, it is desirable to develop a strategy to improve the electrical conductivity of $CuInTe_2$ and simultaneously suppress its lattice thermal conductivity.[4,12] In this work, we find that Mn is a desired doping element to improve both the electrical and thermal transport properties of $CuInTe_2$. Through replacing part of In with Mn, the electrical conductivity of the $CuIn_{1-x}Mn_xTe_2$ sample increases dramatically since Mn element acts as the acceptor to provide additional charge carriers (hole). Meanwhile, the elemental substitution leads to obviously reduced lattice thermal conductivity due to the enhanced phonon scattering. Therefore, enhanced thermoelectric performance is obtained for $CuIn_{1-x}Mn_xTe_2$, resulting from synergistic effect of optimized electrical conductivity and reduced lattice thermal conductivity.

2. Experimental section

Polycrystalline samples of $CuIn_{1-x}Mn_xTe_2$ ($x = 0$, 0.025, 0.05, 0.075, 0.1) were synthesized by a melt-annealing method. The starting materials Cu (99.99%, shot), In (99.999%, shot), Mn (99.999%, piece), Te (99.999%, shot) were weighed according to the stoichiometric ratio and sealed

*Project supported by the National Natural Science Foundation of China (Nos. 51632005 and 51371194) and National Basic Research Program of China (Grant No. 2013CB632500).

†Corresponding author. E-mail: junluo@shu.edu.cn

‡Corresponding author. E-mail: wqzhang@t.shu.edu.cn

© 2017 Chinese Physical Society and IOP Publishing Ltd

in evacuated quartz tubes, which were heated to 1173 K at a rate of 1 K/min and held at this temperature for 24 h. Then, the samples were slowly cooled to 923 K, annealed at 923 K for 72 h, and cooled to room temperature in the furnace. Finally, to obtain densified bulk samples, the as-prepared ingots were crushed into fine powders and then vacuum sintered in a hot-pressing furnace at 823 K for 15 min under an axial pressure of 65 MPa.

Phase identification and structure analysis were carried out by x-ray powder diffraction (XRD) using a Rigaku D/max 2200 diffractometer equipped with Cu-$K\alpha$ radiation (45 kV, 250 mA). The microstructures of the polished hot-pressed samples were investigated by scanning electron microscope (Zeiss Supra 55, Germany). An electron energy x-ray dispersive spectroscopy (EDXS, Oxford) was equipped for elemental mapping and point analysis. The density D of hot-pressed samples was determined by the Archimedes' method and found to be over 97% of the theoretical density. The heat capacity $C_{\rm P}$ was obtained using Dulong–Petit model, $C_{\rm P} = 3nR/M$, where n is the number of atoms per formula unit, R is the gas constant, and M is the molar mass. Thermal diffusivity (λ) was measured by the laser flash method using a Netzsch LFA457 instrument. The thermal conductivity was calculated from the equation $\kappa = C_{\rm P}D\lambda$. The resistivity ρ and Seebeck coefficient S were measured via four probe method utilizing ZEM-3 instrument (ULVAC, Japan) under low-pressure helium atmosphere. The room-temperature carrier concentrations of the samples were obtained from Hall coefficient measurements, which were conducted on a mini cryogen free measurement system (Cryogenic Limited, UK).

3. Results and discussion

Figure 1(a) shows the XRD patterns of $CuIn_{1-x}Mn_xTe_2$ samples ($x = 0$, 0.025, 0.05, 0.075, 0.1). For all these samples, their diffraction peaks can be solely indexed to the chalcopyrite phase (PDF# 81-1937) and no impurities are observed. All the XRD patterns were analyzed by Rietveld refinement. The obtained lattice parameters of the a-axis are shown in Fig. 1(b). It can be seen that the lattice parameter, a, linearly decreases with the Mn contents when $x < 0.075$, indicating the replacement of In^{3+} (0.80 Å) by smaller Mn^{2+} (0.67 Å). Higher Mn content did not lead to further decrease in a, ascribed to the solid solubility limit of Mn.

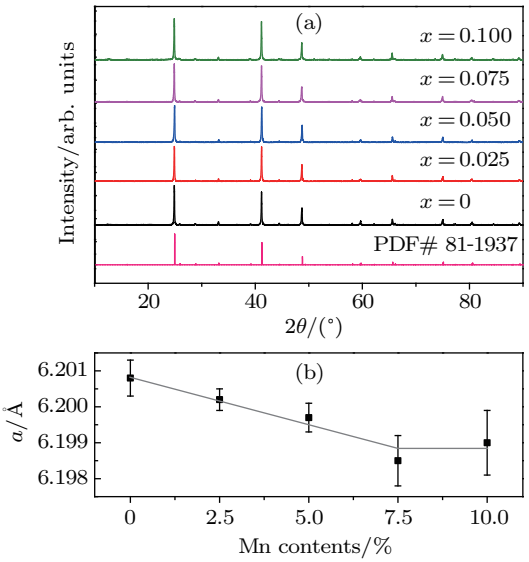


Fig. 1. (color online) (a) The XRD patterns and (b) lattice parameters of the a-axis for $CuIn_{1-x}Mn_xTe_2$ ($x = 0$, 0.025, 0.05, 0.075, 0.1) samples. The gray line in panel (b) is guide for eyes.

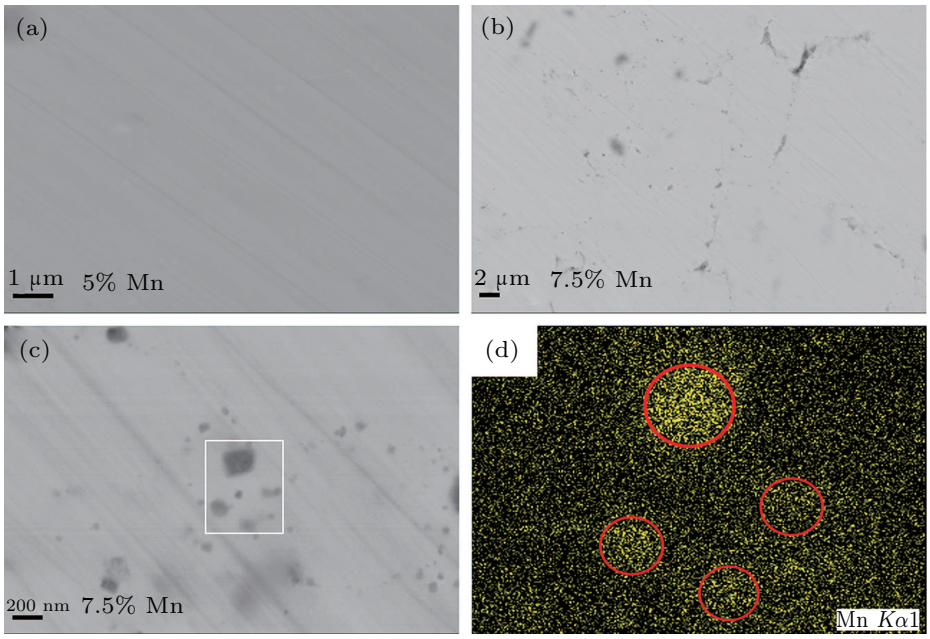


Fig. 2. (color online) BSE images of the samples with (a) 5% Mn and (b) 7.5% Mn. The magnified image of 7.5% Mn sample and Mn elemental mapping of boxed area are shown in panels (c) and (d), respectively.

Figure 2 presents the backscattered electron (BSE) microscopy of the polished surface for typical samples with x = 0.05 and 0.075. As shown in Fig. 2(a), the BSE image of the sample with 5% Mn reveals a typical homogeneous solid solution microstructure and no obvious second phase precipitates can be found. However, for the sample with 7.5% Mn (see Figs. 2(b) and 2(c)), particle-like precipitates with sizes from several to 200 nm can be clearly observed, which are randomly distributed in the $CuInTe_2$ matrices. Thus, we can conclude that the solubility of Mn is between 5% and 7.5%. The precipitates cannot be identified in the XRD patterns, possibly due to their low content and tiny size. The elemental mapping (Fig. 2(d)) reveals that the precipitates have Mn-rich compositions.

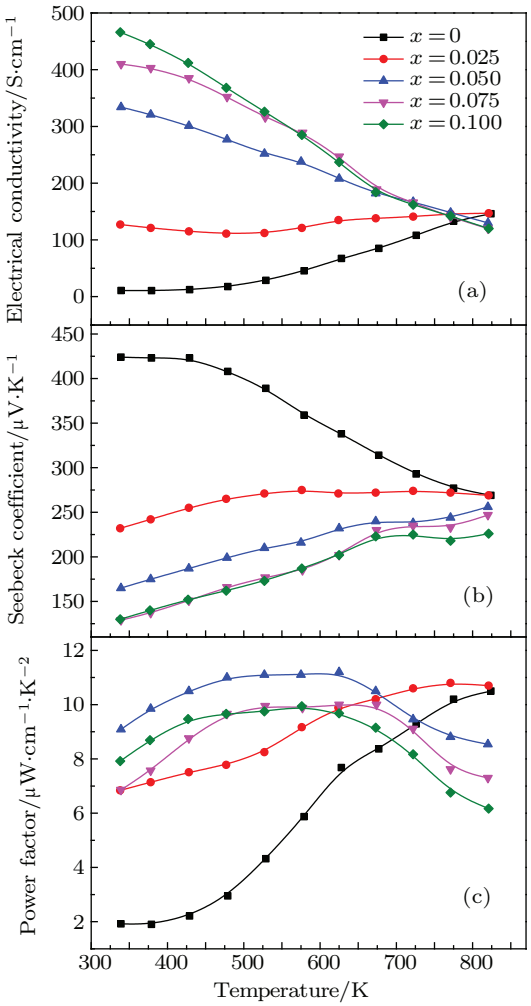


Fig. 3. (color online) The temperature dependence of (a) electrical conductivity, (b) Seebeck coefficient, (c) power factor for $CuIn_{1-x}Mn_xTe_2$ ($x = 0$, 0.025, 0.05, 0.075, 0.1) samples.

The electrical transport properties for $CuIn_{1-x}Mn_xTe_2$ samples ($x = 0$, 0.025, 0.05, 0.075, 0.1) are compared in Fig. 3. As shown in Fig. 3(a), the electrical conductivity of the pristine $CuInTe_2$ sample increases with the rising temperature, exhibiting the typical behavior of intrinsic semiconductors. However, when Mn is doped, the room-temperature electrical conductivities of $CuIn_{1-x}Mn_xTe_2$ are dramatically increased, and the temperature dependence of conductivities becomes the behavior of degenerate semiconductors, indicating that the carrier concentrations of the samples were substantially enlarged by Mn doping. The measured room-temperature hole concentrations (n_h) and Hall mobilities of carriers (μ_H) for the $CuIn_{1-x}Mn_xTe_2$ samples are listed in Table 1. It can be seen that the hole concentrations of the samples increase with the increase of Mn contents. It has been reported that the hole concentration of the Mn-free $CuInTe_2$ is about 5.75×10^{18} cm^{-3}.[12] Consequently, the room-temperature electrical conductivity of the sample with $x = 0.1$ is $\sim$46600 S/m, which is more than 40 times larger than that of the sample free of Mn (about 1100 S/m). Furthermore, the increasing of the hole concentrations suppresses the intrinsic excitation of charge carriers. Thus, the occurrence of bipolar conduction is pushed to higher temperatures with increasing Mn contents.

Table 1. Room temperature hole concentrations (n_h) and Hall mobilities of carriers (μ_H) for the $CuIn_{1-x}Mn_xTe_2$ ($x = 0.025$, 0.05, 0.075, 0.1) samples.

x	0.025	0.05	0.075	0.1
n_h/cm^{-3}	7.4×10^{18}	6.0×10^{19}	8.3×10^{19}	1.8×10^{20}
μ_H/cm^2·V^{-1}·s^{-1}	75	38	30	33

Figure 3(b) shows the temperature-dependent Seebeck coefficient of $CuIn_{1-x}Mn_xTe_2$ samples. Positive Seebeck coefficients reveal the p-type hole dominant conduction in all the samples. The variation trend of the Seebeck coefficient with temperatures is opposite to that of the electrical conductivity. The Seebeck coefficient of the pristine $CuInTe_2$ sample decreases with the temperature increasing, further proving that the undoped sample is a non-degenerate semiconductor, whereas the Seebeck coefficient for the samples doped with Mn increases with the temperature increasing, exhibiting a behavior of degenerate semiconductors. As the Mn content increases, the Seebeck coefficients at 340 K reduce from 424 μV/K for the pristine sample to 130 μV/K for the sample with $x = 7.5\%$. The Seebeck coefficients for the samples with $x = 0.075$ and 0.1 were found to be almost identical at lower temperature range. One possible reason is that the solid solubility of Mn in $CuInTe_2$ is below 0.075. The increased electrical conductivity and moderately decreased Seebeck coefficients lead to enhanced power factors (PF) in the temperature rangingfrom room temperature to 720 K (Fig. 3(c)). A maximum PF of 11.2 μV·cm^{-1}·K^{-2} at 625 K is achieved for the sample with $x = 0.05$, which is much larger than that for $CuInTe_2$ at 625 K.

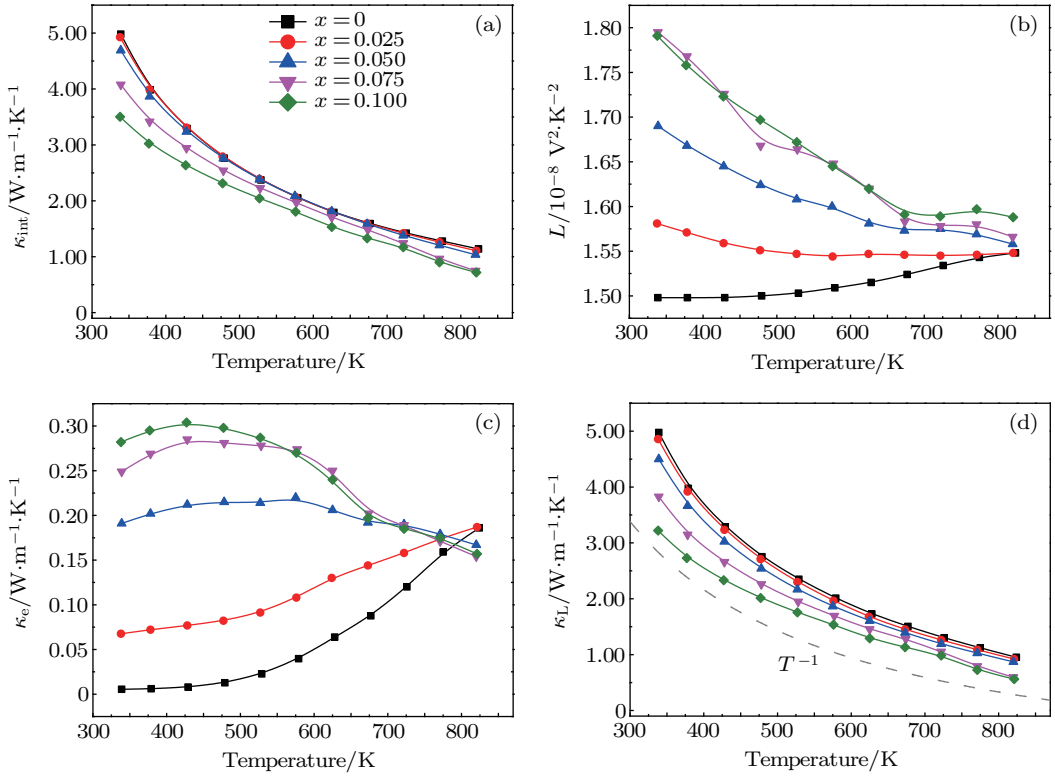


Fig. 4. (color online) The temperature dependence of (a) total thermal conductivities, (b) Lorentz numbers, (c) electronic thermal conductivities, and (d) lattice thermal conductivities for $CuIn_{1-x}Mn_xTe_2$ ($x = 0$, 0.025, 0.05, 0.075, 0.1) samples. The dashed line in panel (d) is the curve for T^{-1} relationship.

Figure 4 depicts the temperature-dependent thermal transport properties of the samples. As shown in Fig. 4(a), the introduction of Mn can substantially reduce the total thermal conductivities ($\kappa_{\rm tot}$). Lattice thermal conductivity ($\kappa_{\rm L}$) can be obtained from $\kappa_{\rm tot}$ by subtracting the electronic part ($\kappa_{\rm e}$) according to the relationship of $\kappa_{\rm tot} = \kappa_{\rm L} + \kappa_{\rm e}$. Electronic thermal conductivity $\kappa_{\rm e}$ can be calculated from the electrical conductivity by the celebrated Wiedemann–Franz law $\kappa_{\rm e} = L\sigma T$, where L is the Lorenz number.[17] The Lorenz number in degenerate semiconductors can be calculated by Seebeck coefficient within a single parabolic model, using the following equations:[18]

$$S = \frac{k_{\rm B}}{e}\left(\frac{2F_1(\eta)}{F_0(\eta)} - \eta\right), \tag{1}$$

$$L = \left(\frac{k_{\rm B}}{e}\right)^2 \frac{3F_0(\eta)F_2(\eta) - 4F_1(\eta)^2}{F_0(\eta)^2}, \tag{2}$$

where $k_{\rm B}$, e, and η are the Boltzmann constant, electron charge, and reduced Fermi energy (Fermi energy divided by $k_{\rm B}T$), respectively, and $F_n(\eta)$ is the n-th Fermi–Dirac integral. The Lorenz number (L) can be calculated using Eq. (2) with the values of η, which are fitted from the experimental data of Seebeck coefficients by Eq. (1). The calculated Lorenz numbers and related electronic thermal conductivities of all the samples are illustrated in Figs. 4(b) and 4(c), respectively. It can be derived from Fig. 4(c) that $\kappa_{\rm e}$ increases with the increase of Mn contents (i.e., electrical conductivities). Consequently, the large reduction in $\kappa_{\rm tot}$ mainly comes from the decreased $\kappa_{\rm L}$ (see Fig. 4(d)), which can be ascribed to the addition of Mn. It can be seen in Fig. 4(d) that $\kappa_{\rm L}$ of all the samples approximately follow a T^{-1} relationship (the dashed line in Fig. 4(d)), indicating that the dominant phonon scattering mechanism should be the three-phonon Umklapp scattering process (U-process).[19] The incorporation of Mn can introduce a large number of point defects that can scatter short-wavelength phonons and thus mainly decrease the high-temperature lattice thermal conductivities. Additionally, nanosized precipitates occurring in samples with higher Mn concentrations can provide extra phonon scattering center for mid-wavelength phonons, which can effectively reduce the lattice thermal conductivities near room temperatures. The further reduced $\kappa_{\rm L}$ at lower temperatures for samples with $x = 0.075$ and 0.1 can be attributed to their additional nanosized precipitates.

The temperature-dependent dimensionless thermoelectric figure-of-merit ZT of $CuIn_{1-x}Mn_xTe_2$ compounds is calculated based on the above transport data and is plotted in Fig. 5. The ZT values increase when approaching high temperature, and reach a maximum value of ~ 0.8 at 813 K for the sample with $x = 0.075$, which is slightly higher than that of the pristine $CuInTe_2$ sample. Nevertheless, the average ZT is also an important factor for actual thermoelectric applications.[20] The calculated average ZT for all the samples is shown in the inset of Fig. 5. It can be seen that the average ZT of all the samples with Mn incorporation is much higher than that of the pristine one and is up to 0.34 for the samples with $x = 0.075$ and 0.1,

owing to their moderate power factors and low lattice thermal conductivities in lower temperature range.

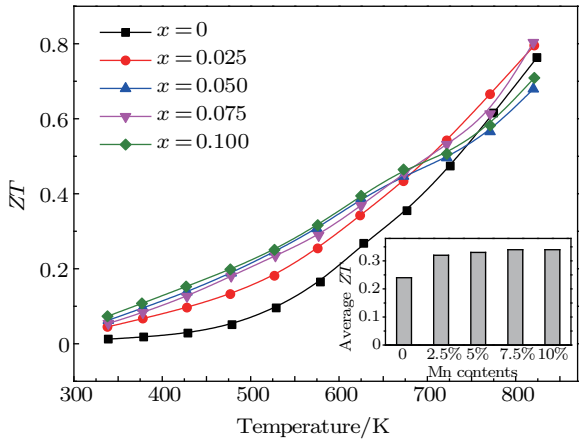


Fig. 5. (color online) Influence of Mn contents on figure of merit ZT for $CuIn_{1-x}Mn_xTe_2$ samples. The inset is the average ZT calculated from the integration using the formula $ZT_{\text{average}} = \int_{T_1}^{T_2} ZT\mathrm{d}T/(T_2-T_1)$.

4. Conclusion

In summary, polycrystalline chalcopyrite $CuIn_{1-x}Mn_xTe_2$ compounds ($x = 0$, 0.025, 0.5, 0.075, 0.1) has been successfully synthesized. The solubility of Mn in $CuInTe_2$ is determined to be below 7.5%. By substituting In, Mn acts as an effective acceptor dopant and can dramatically improve the electrical transport properties of the pristine $CuInTe_2$ system. In addition, κ_L of the $CuInTe_2$ system can be substantially decreased by the point defects and nanosized precipitates introduced by the incorporation of Mn, and thus resulting in a considerably reduction in κ_{tot}. As a result, an enhanced average ZT value up to 0.34 is achieved for sample $CuIn_{0.925}Mn_{0.075}Te_2$, which is 41% higher than that of the undoped $CuInTe_2$, making it a promising candidate for thermoelectric applications. Furthermore, it is reported that anions (P^{3-}, Sb^{3-}) doping on the Te sites can effectively increase the Seebeck coefficient and consequently enhance the PF of the system.[4] Thus, introducing anion dopants plus some additional microstructure engineering in our Mn-doped $CuInTe_2$ system may bring its ZT value to that of the state-of-the-art thermoelectric materials.

References

[1] Zhao L D, Lo S H, Zhang Y, Sun H, Tan G, Uher C, Wolverton C, Dravid V P and Kanatzidis M G 2014 *Nature* **508** 373

[2] Liu H, Shi X, Xu F, Zhang L, Zhang W, Chen L, Li Q, Uher C, Day T and Snyder G J 2012 *Nat. Mater.* **11** 422

[3] Pei Y, Shi X, LaLonde A, Wang H, Chen L and Snyder G J 2011 *Nature* **473** 66

[4] Luo Y, Yang J, Jiang Q, Li W, Zhang D, Zhou Z, Cheng Y, Ren Y and He X 2016 *Adv. Energy Mater.* **6** 1600007

[5] Luo Y, Yang J, Jiang Q, Li W, Xiao Y, Fu L, Zhang D, Zhou Z and Cheng Y 2015 *Nano Energy* **18** 37

[6] Kucek V, Drasar C, Kasparova J, Plechacek T, Navratil J, Vlcek M and Benes L 2015 *J. Appl. Phys.* **118** 125105

[7] Hu C, Peng K, Wang G, Lijie Guo, Wang G and Zhou X 2015 *Mater. Res. Soc. Symp. Proc.* **1735**

[8] Carr W D and Morelli D T 2015 *J. Alloys Compd.* **630** 277

[9] Zhang J, Liu R, Cheng N, Zhang Y, Yang J, Uher C, Shi X, Chen L and Zhang W 2014 *Adv. Mater.* **26** 3848

[10] Cheng N, Liu R, Bai S, Shi X and Chen L 2014 *J. Appl. Phys.* **115** 163705

[11] Cui J, Li Y, Du Z, Meng Q and Zhou H 2013 *J. Mater. Chem. A* **1** 677

[12] Liu R, Xi L, Liu H, Shi X, Zhang W and Chen L 2012 *Chem. Commun.* **48** 3818

[13] Kosuga A, Plirdpring T, Higashine R, Matsuzawa M, Kurosaki K and Yamanaka S 2012 *Appl. Phys. Lett.* **100** 042108

[14] Plirdpring T, Kurosaki K, Kosuga A, Day T, Firdosy S, Ravi V, Snyder G J, Harnwunggmoung A, Sugahara T, Ohishi Y, Muta H and Yamanaka S 2012 *Adv. Mater.* **24** 3622

[15] Yusufu A, Kurosaki K, Kosuga A, Sugahara T, Ohishi Y, Muta H and Yamanaka S 2011 *Appl. Phys. Lett.* **99** 061902

[16] Wang H X, Ying P Z, Yang J F, Chen S P and Cui J L 2016 *Acta Phys. Sin.* **65** 067201 (in Chinese)

[17] Cao B L, Jian J K, Ge B H, Li S M, Wang H, Liu J and Zhao H Z 2017 *Chin. Phys. B* **26** 017202

[18] Biswas K, He J Q, Blum I D, Wu C I, Hogan T P, Seidman D N, Dravid V P and Kanatzidis M G 2012 *Nature* **489** 414

[19] Goldsmid H J 2010 *Introduction to Thermoelectricity* (Berlin, Heidelberg: Springer-Verlag) pp. 37–38

[20] Zhang Y, Wu L H, Zhang J Y, Xing J J and Luo J 2016 *Acta Mater.* **111** 202